The University of Chicago
Chicago, Illinois
Advisor: Prof. Jonathan Simon
June 2017

Holographic Reconstruction of the Chern Invariant of a Photonic Landau Level

Michelle Chalupnik

Submitted in partial fulfillment of the requirements for the degree of
Bachelor of Arts with Honors in Physics

Abstract

In 2016, Schine et al [1] demonstrated photonic Landau levels in a twisted four-mirror optical cavity, showing an analogue of the quantum Hall effect for photons. For my undergraduate senior thesis, I constructed a twisted four-mirror optical cavity, and worked with graduate student Nathan Schine to measure the Chern invariant of the lowest Landau level of this system. We use a formalism introduced by Kitaev to find the Chern number in real space, rather than momentum space [2]. By imposing a lattice on the transverse cavity plane, injecting light into the cavity along each lattice site, and imaging and then using holography to reconstruct the electric fields outputted from the cavity, we find for our lowest photonic Landau level a Chern number of $1.08 - 0.12i$. A second measurement using smaller grid spacing yields a Chern number of $0.93 - 0.10i$. Both experimentally found Chern numbers are close to the expected value of 1.

Acknowledgements

Warmest thanks to professor Jonathan Simon and graduate student Nathan Schine for giving me this project, answering questions even when I asked the same question twice (or more times), helping me, working on this project alongside me, and basically being amazing mentors. I also want to thank the rest of the Simon lab. You are all the coolest people and it has been an honor to work with you. I would also like to acknowledge and thank the University of Chicago physics undergraduate honors thesis program for providing the opportunity to write this thesis.

Contents

Chapter 1

Introduction

In this section, I will review the aspects of theory important for understanding this experiment. First and foremost, the quantum Hall effect with electrons is explained and the quantization of Hall conductivity is derived. Next, the mathematical definition of the Chern number is explained, and related to Berry phase. Then, the connection between the Chern number and the quantum Hall effect with electrons is briefly touched on. Following that, Kitaev's real-space Chern number formulation (and the formulation experimentally used) is introduced. Then the basis for our photonic analogue to the quantum Hall effect using our experimental system is established, and our system is compared to the traditional quantum Hall effect.

1.1 Integer Quantum Hall Effect

The integer quantum Hall effect revealed that the Hall conductance of a conductor in a magnetic field is quantized [3, 4]. In this section, I discuss how to find the energy solutions to the quantum Hall effect Hamiltonian, and how to derive quantization of the Hall conductance.

In the integer quantum Hall effect, a current of electrons is sent through a thin conductor extending as a plane (see Figure 1.1a) with very long length along the x and y axes, but thin length along the z axis. A magnetic field B is then applied perpendicular to the conductor's

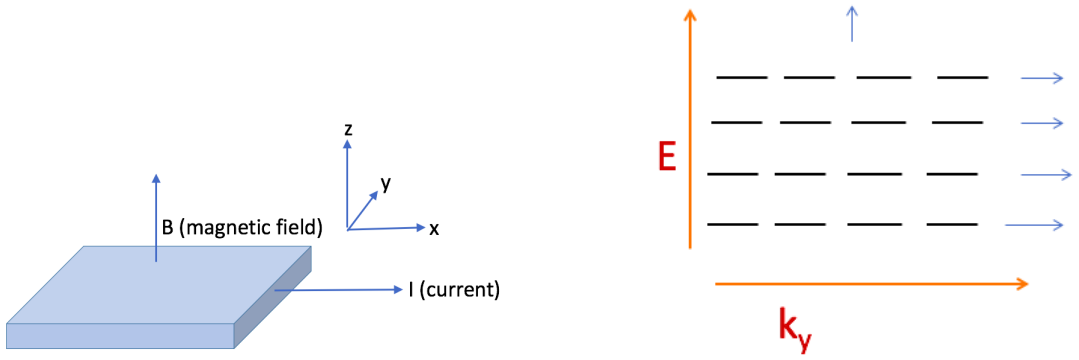

(a) (b)

Figure 1.1: (a) A simple drawing of the basic elements of the quantum Hall effect. A current is sent through a thin conductor, and a magnetic field is applied perpendicular to the conductor's surface. (b) A cartoon drawing of the energy level solutions, also called Landau levels, in the quantum Hall effect. The energy levels are evenly spaced vertically and highly degenerate with k_y.

surface. We can write the sum of the forces experienced by an electron moving in the current as

$$\vec{F} = -e\vec{v} \times \vec{B} \tag{1.1}$$

We can define a quantity called the Hall resistance, R_H, where $R_H \equiv V_y/I_x$. V_y is the voltage difference along the y-axis, and I_x is the current along the x-axis. Note that R_H is not the usual definition of resistance, but instead defined by the voltage drop perpendicular to the current, instead of parallel to the current. We can then define Hall resistivity with respect to the area $(A = L_x \cdot L_y)$ and length (L_x) as $\rho_H = (R_H A)/(L)$ and Hall conductivity as $\sigma_H = 1/\rho_H$.

A critical finding of the integer quantum Hall effect was that the Hall conductivity is quantized, with

$$\sigma_H = \frac{\nu e^2}{h}, \tag{1.2}$$

where h is Planck's constant, e is the charge on an electron, and ν is an integer, also known as the filling factor.

To derive the quantization of Hall conductance, we begin by writing down the Hamiltonian for

an electron in a magnetic field [5, 3]

$$H = \frac{(\vec{P} - e\vec{A})^2}{2m} \tag{1.3}$$

We work in the Landau gauge, and set $\vec{A} = (0, Bx, 0)$, to satisfy $\nabla \times \vec{A} = B\hat{z}$. We also assume the conductor is thin enough so that the electrons do not travel in the z direction, so that $P_z = 0$. We can then write

$$H = \frac{P_x^2}{2m} + \frac{(P_y - eBX)^2}{2m}$$

Diagonalizing P_y and H separately, we write

$$\psi(x, y) = \psi_x(x) \cdot e^{ik_y y}$$
$$H = \frac{P_x^2}{2m} + \frac{e^2B^2}{2m}\left(\frac{\hbar k_y}{eB} - X\right)^2$$

Like a quantum harmonic oscillator, the Hamiltonian has the solutions

$$E_\nu = (\nu + \frac{1}{2})\hbar\omega_c, \qquad \text{where} \qquad \omega_c \equiv \frac{eB}{m} \tag{1.4}$$

This gives an energy spectrum of equally spaced energy levels, each of which are highly degenerate across different values of k_y (see Figure 1.1b). When there is no limit on the number of electrons that can flow (as is the case in our system because it is connected to a voltage source), the energy levels are filled up to the Fermi energy, so the energy will be an integer multiple of the degeneracy of the energy levels.

The degeneracy is determined by the physical dimensions of the conductor. As we saw from the Hamiltonian, the wave function along the x-axis is centered around $\hbar k_y/eB$, so $\hbar k_y/eB$ can't be larger than L_x, the length of the conductor in the x direction. But we also know because of boundary conditions, k_y is quantized like a particle in a box ($k_y = 2\pi n/L_y$). The largest

possible value for n, and thus the degeneracy of each Landau level, is therefore

$$n = \frac{L_y k_y}{2\pi} = \frac{L_y}{2\pi}\frac{L_x eB}{\hbar} = \frac{L_y L_x eB}{h}$$

After finding the degeneracy, showing the quantization of the Hall conductivity is fairly straightforward. Assuming steady state, where an E field builds up along the y axis due to the buildup of potential perpendicular to the current, $v = E_y/B$, so

$$\frac{1}{\sigma_H} = \rho_H = \frac{L_y}{L_y}\frac{V_y}{I_x} = \frac{L_y E_y}{(\frac{n\nu}{L_y L_x})evL_y} = \frac{h}{\nu e^2}$$

The quantum Hall effect is not only interesting for the quantization of Hall conductance, but also for the significant role "edge modes" play for quantum Hall conductors. A crude way to picture edge modes in the integer quantum Hall effect is to picture each electron on the surface of the conductor moving in circles because of the perpendicular magnetic field. The electron has an orbital radius equal to the magnetic length, $l_B = \sqrt{\hbar/eB}$ (note that the cyclotron radius is mv/qB, and angular momentum rmv is quantized by $\hbar$). The number of cyclotron orbits is equal to the degeneracy of the Landau level. Current is only allowed to flow along the edges of the conducting surface, since currents flowing in one direction are canceled by neighboring currents flowing in the opposite direction (see Figure 1.2, left). The resulting edge mode actually orbits opposite the direction of the cyclotron orbits, and hence are counter-propagating (see Figure 1.2, right).

1.2 Mathematical Definition of the Chern Number

The Chern number is a topological invariant that has applications in many areas of physics, including solid state physics. The Chern number is an integer equal to the Berry curvature F_{ij}, integrated over a two-dimensional, toroidal parameter space, λ_i, λ_j [4, 6]

$$C = \frac{1}{2\pi}\int_{S_{ij}} F_{ij} d^2\lambda^{ij}, \tag{1.5}$$

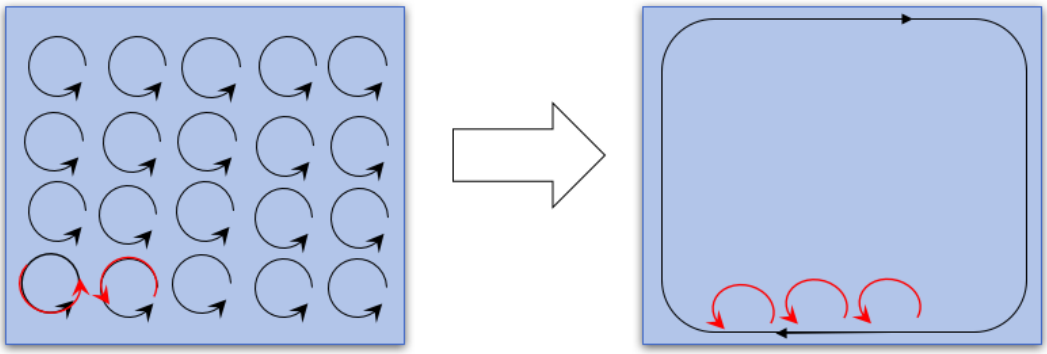

Figure 1.2: On left: electrons are moved by the magnetic field to travel in circles, but current traveling in the center cancels itself. This is shown explicitly for one small portion with the red arrows. On right: the cyclotron orbits on the edges (in red) create counter-propagating edge modes (in black).

where F_{ij}, the Berry curvature, is equal to the curl of the Berry connection in parameter space λ^{ij} [4]

$$F_{ij} = -i\left(\frac{\partial}{\partial\lambda_i}\langle\psi|\frac{\partial\psi}{\partial\lambda_j}\rangle - \frac{\partial}{\partial\lambda_j}\langle\psi|\frac{\partial\psi}{\partial\lambda_i}\rangle\right)$$

To understand the physical meaning of the Chern number, it is best to start from the adiabatic theorem. The adiabatic theorem states that if you begin in an eigenstate ψ of a Hamiltonian H, and very slowly ("adiabatically") modify your system so that it ends up in a different Hamiltonian H', the system will never at any given point in time change eigenstates, but will instead end up in ψ', the eigenstate of H' that corresponds to the eigenstate ψ in H [5]. As an example, if you start with a particle in a box in an eigenstate ψ_3 with two nodes, and slowly push in one wall of the box until the box is (for instance) half as long as it initially was, the ending eigenstate will be ψ_3', where ψ_3' is the two-nodal eigenstate of the shorter box.

According to the adiabatic theorem, although very slowly changing the Hamiltonian preserves the eigenstate, the transition can introduce a phase that differentiates the system from other systems that did not undergo adiabatic transformations. This phase is called the Berry phase [7]. The Berry phase between some initial eigenstate ψ_n and some ending eigenstate ψ_n' can be derived by writing the ending eigenstate ψ_n' as a linear combination of the initial eigenstates

ψ_m, applying the Schrödinger equation, and taking the limit where dH/dt, the change of the Hamiltonian in time, is negligibly small [5]. The result (after changing variables from time t to some arbitrary parameter λ^i) is that the phase difference between the adiabatically transformed eigenstate ψ'_n and an identical eigenstate that has not undergone an adiabatic transformation $\psi'_{n,0}$ is, in terms of the initial wave function ψ_n,

$$\psi'_{n,0} = e^{i\gamma_n}\psi'_n$$

with

$$\gamma_n \equiv i \int \langle\psi_n|\frac{\partial}{\partial\lambda^i}|\psi_n\rangle \, d\lambda^i.$$

For ease of notation, we define the Berry connection A_i to be

$$A_i \equiv -i \langle\psi_n|\frac{\partial}{\partial\lambda^i}|\psi_n\rangle$$

Given a two-dimensional parameter space with parameters λ_i and λ_j, one can define the Berry curvature, F_{ij}, as the curl of the Berry connection.

$$F_{ij} \equiv \nabla \times A_{ij} = \frac{\partial A_i}{\partial\lambda_j} - \frac{\partial A_j}{\partial\lambda_i} = -i\left(\frac{\partial}{\partial\lambda_i}\langle\psi_n|\frac{\partial}{\partial\lambda^j}|\psi_n\rangle - \frac{\partial}{\partial\lambda_j}\langle\psi_n|\frac{\partial}{\partial\lambda^i}|\psi_n\rangle\right)$$

It is useful to think of the Berry curvature as playing a very similar role to the Berry connection as magnetic fields play to vector potentials ($\vec{B} = \nabla \times \vec{A}$). For both the Berry connection and for vector potentials, taking the curl gets rid of gauge freedom, and so results in a more physical quantity.

A mathematical fact involving the Gauss-Bonnet theorem is that the integral of the Berry curvature of a wavefunction over a torus-shaped two-dimensional parameter space (a parameter space periodic in both parameters) is quantized in integer multiples of 2π (see Equation 1.5). The quantization integer, C, is also called the Chern number [4]. I only cite the result, and give as sources pages 58-60 of Tong [4], page 8 of Kane [6], and Chern's proof [8].

1.3 Chern Number and the Integer Quantum Hall Effect

A Chern number can be defined for an energy band (including but not limited to Landau levels) in a quantum Hall system. Significantly, the sum of the Chern numbers C_α over the filled bands α equaled the filling factor ν. and hence, is related to the Hall conductivity (recall equation 1.2) by the equation

$$\sigma_H = -\frac{e^2}{h}\sum_\alpha C_\alpha. \tag{1.6}$$

This is also known as the TKNN formula, after the initials of the scientists who first wrote about it [9].

Deriving the TKNN formula is not trivial (see pages 54-56, 63-64 of Tong [4], pages 107-108 of Prange and Girvin [10]). One can add a perturbative term to a Hamiltonian describing electrons on a conducting surface, $\Delta H = -\vec{J}\cdot\vec{A}$. Note that the perturbative term only includes the electric field required to begin the initial current flow of electrons in the $\hat{x}$ direction; it does not include the magnetic field (despite the presence of $\vec{A}$, $\vec{A}$ is only used in a context where $\vec{E} = -\partial_t\vec{A}$). One can write $\vec{A}$ in terms of frequency, use linear response theory to write the expectation value of the current, and perform an integral over complex time to obtain the Kubo formula for Hall conductivity. From the Kubo formula, more approximations and algebra lead to a formula for Hall conductivity which should look familiar: [4, 10]

$$\sigma_H = \frac{ie^2}{\hbar}\sum_\alpha \int_{T^2} \frac{d^2\vec{k}}{(2\pi)^2} \langle\partial_{k_y}\psi_k^\alpha|\partial_{k_x}\psi_k^\alpha\rangle - \langle\partial_{k_x}\psi_k^\alpha|\partial_{k_y}\psi_k^\alpha\rangle \tag{1.7}$$

In the equation above, we integrate over T^2, the Brillouin torus, described by momentum wave-vectors $\vec{k}$. α enumerates all of the filled bands. ψ_k^α are the wavefunctions described by each momentum vector.

A Brillouin torus is defined by the allowed momentum in a lattice [11]. Just as the periodic potential restricts the location of a wave-function in real-space, it also restricts the location in momentum-space. Using Bloch's theorem and the Kronig-Penney model, one can discover that

in a one-dimensional lattice, there are regions of forbidden energy, or "band gaps," while energy is periodic with momentum instead of quadratic. A unit-cell of the periodic momentum-space is called the Brillouin zone. In solid state physics, a conductor can be considered to be a two-dimensional lattice of ions, and electrons in the conductor exist in a momentum-space periodic in both k_x and k_y. The Brillouin zone can be envisioned as a rectangle periodic along both its length and its height, and just as one can connect the two ends of a periodic line segment to make a circle, one can connect the two pairs of edges of a rectangle to make a torus. For this reason, the Brillouin zone is topologically equivalent to a torus.

We see that equation 1.7 is essentially identical to equation 1.6, showing that the integral of the Berry curvature of the quantum Hall wavefunctions over the Brillouin torus equals the Chern number, which equals the filling factor.

Interestingly, this definition of Hall conductivity does not necessarily require Landau levels, but any energy bands that can be defined and integrated over with respect to a toroidal parameter space. In fact, non-zero Chern numbers have been observed for energy bands in a hexagonal lattice system with no Landau levels, based purely on the periodic structure of the potential [12].

1.4 Calculating the Chern Number in Real Space

In 2006, Alexei Kitaev introduced a formalism for computing the Chern number of a disordered band in real space [2]. I will only cite the results here, explain the formula, and attempt to give a vague justification. We begin by imposing a lattice on the real space of a quantum Hall system band, even if no physical lattice may be present. The lattice spacing must be at least as small as the magnetic length. Additionally, a lattice size that is small compared to the bulk will make it more likely the sum will converge to the Chern number[13], as we wish to avoid the edge modes with opposite circulation.

Recall that a quantum mechanical projector projects one eigenstate onto another eigenstate or subspace of eigenstates. We construct a projector P^{μ} that projects the excitation at a given

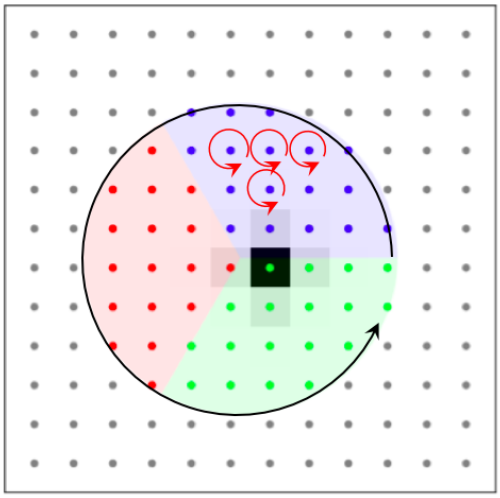

Figure 1.3: In this drawing taken from Ma et al [13], a lattice is imposed on the electric fields outputted from the cavity tuned to a single Landau level. The lattice is divided into three sections, A, B, and C (represented by three different colors). Matrix elements of a band projector P^μ on this lattice can be used to find the Chern number [2, 13]. The red arrows I have added show the individual "current" circulation, while the black arrow I have added shows the additive total "current" circulation (compare to Figure 1.2).

lattice site onto an energy band μ. We wish to apply this projector operator between each lattice site i and j. The matrix elements of P^μ are given by [13]

$$P^\mu_{ij} = \langle i|P^\mu|j\rangle = \langle i| \left[\sum_{n\in \text{Band}\mu} |n\rangle \langle n| \right] |j\rangle \tag{1.8}$$

In the equation above, μ denotes an energy band, and $|n\rangle$ are eigenstates within the band. After imposing the lattice, one divides the lattice into three regions. In Figure 1.3, these three regions are represented as three colors, red, blue, and green, and in equation 1.9 below, they are regions A, B, and C, respectively. We find the matrix elements for each propagator that circulates clockwise (matrix elements between blue and green, green and red, or red and blue lattice sites) and for each propagator that circulates counter-clockwise (matrix elements between blue and red, red and green, or green and blue lattice sites). The sum of the difference of the products of the clockwise-circulating projectors minus the products of the counterclockwise-circulating projectors on each lattice site equals the Chern number[13]

$$C^\mu = 12\pi i \sum_{\alpha\in A,\beta\in B,\gamma\in C} \left(P^\mu_{\alpha\beta}P^\mu_{\beta\gamma}P^\mu_{\gamma\alpha} - P^\mu_{\alpha\gamma}P^\mu_{\gamma\beta}P^\mu_{\beta\alpha}\right) \tag{1.9}$$

As a vague justification, note that Kitaev's formalism for finding the Chern number intuitively corresponds well with the crude picture of cycling electrons we mentioned at the end of section 1.1. In Figure 1.3, one can see that we expect the circulating currents to cancel where not along the edge of the measurement. However, unlike in Figure 1.2, as long as we measure in the bulk, we will not include a counter-propagating edge mode. If a counter-propagating edge mode is included, we will measure a Chern number of zero with this formalism.

1.5 Photonic Landau Levels in a Photonic Quantum Hall Effect

Using a special optical cavity (a collection of mirrors trapping laser light), we can create a quantum Hall effect analogue with photons. How can a system with photons, uncharged bosons that are unable to experience Lorentz forces, create an analogue to the quantum Hall effect? In this section we address this question by discussing our photonic Landau levels and the system we use to achieve them.

If we take a two-mirror optical cavity and look at the transverse plane perpendicular to the path of the light, we can view the light as a particle moving in a harmonic trap (see Figure 1.4a). Without the curvature of the mirrors, the light would not be trapped and would eventually bounce out of the cavity; but with the mirror curvature, the transverse light particle feels a harmonic potential.

A harmonic trap is not the only Hamiltonian we can create for a transverse light particle; we can also create a Coriolis and Centrifugal force. Figure 1.4b shows a non-planar four mirror cavity with the mirrors positioned tetrahedrally, the same system used by Nathan Schine, et al. to demonstrate photonic Landau levels [1]. In this optical cavity, we see another effective force acting on our transverse light particles. Each time a photon completes a round trip through the cavity, it is displaced (specifically, rotated) due to the non-planar geometric twist of the cavity (see Figure 1.4b). Viewed in the transverse plane, the transverse light particle rotates as

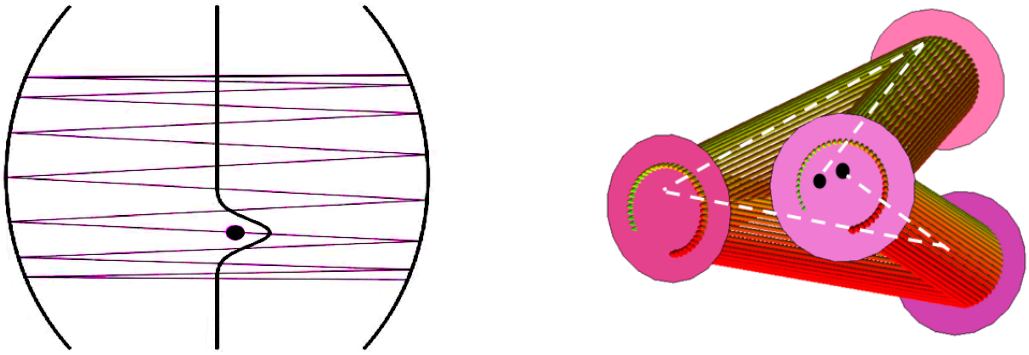

(a) (b)

Figure 1.4: (a) Figure of light trapped between two mirrors. When the light travels away from the mirror centers, the mirror curvature pushes the light back. In the transverse plane, the light experiences a harmonic trap-like potential. (b) A drawing of a non-planar four mirror optical cavity that can result in Coriolis and Centrifugal forces acting on photons. Mirrors are shown as pink disks. The beginning and ending positions of a photon are shown as black spots, and the path the photon takes is shown as a dotted white line. One can see by following the dotted white line that completing one round trip through the cavity rotates the photon in the transverse plane.

if being acted on by Coriolis and Centrifugal forces. Note the similarity of the Coriolis force, $\vec{F} = 2m\vec{v} \times \vec{\Omega}$, to equation 1.1.

We can write a Hamiltonian for the light particles in the transverse plane, and we find that it now looks like a quantum Hall effect Hamiltonian for a charged particle in an electric field, but with an additional trapping term.

$$\begin{aligned} H &= \frac{P_x^2}{2m} + \frac{\left(P_y - 2m\Omega_{\text{rot}}X\right)^2}{2m} - \frac{1}{2}m\Omega_{\text{rot}}^2 r^2 + \frac{1}{2}m\omega_{\text{trap}}^2 r^2 \\ &= \frac{P_x^2}{2m} + \frac{\left(P_y - eB_{\text{syn}}X\right)^2}{2m} + \frac{1}{2}m\omega_{\text{combined}}^2 r^2 \end{aligned}$$

In the equation above, ω_{trap} is a function of the mirror curvature and the length of the cavity, and it can be tuned by adjusting the length of the cavity, while $\vec{\Omega}$ is a fixed parameter of the cavity construction. We define $(e\vec{B})_{\text{syn}} = 2m\vec{\Omega}_{\text{rot}}$. The trapping term due to mirror curvature and the centrifugal term can be absorbed into one term, ω_{combined}, as they are both proportional to r^2.

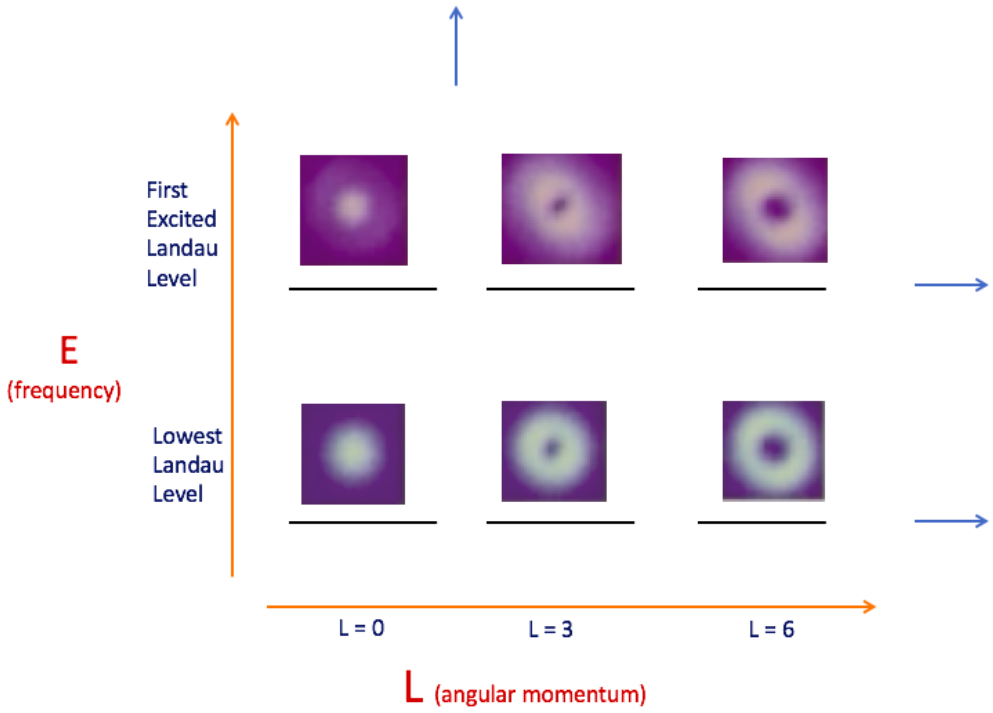

Figure 1.5: A cartoon drawing of the photonic Landau levels possible in a twisted four-mirror cavity at degeneracy. At degeneracy, Laguerre-Gauss modes of varying angular momentum become equal in energy, similar to the degeneracy in k_y in Figure 1.1b.

In fact, by adjusting the cavity length, the trapping term can be tuned to cancel the centrifugal term, leaving a Hamiltonian of the form

$$H = \frac{\left(\vec{P} - e\vec{A}_{\text{syn}}\right)^2}{2m}.$$

This Hamiltonian looks identical to the Hamiltonian in equation 1.3 We can see by the reproduction of an analogous Hamiltonian to the one of the electrons in section 1.1, that the solution to this Hamiltonian will consist of photonic Landau levels, as shown in Figure 1.5. Solving in a different gauge will give the degeneracy across angular momentum instead of across k_y.

Chapter 2

Experiment

2.1 Optical Cavity and Laser Locking Scheme

Our goal is to experimentally measure a Chern number of a photonic Landau level of an optical cavity system nearly identical to the optical cavity system used by Schine, et al, using Kitaev's formalism (as described in section 1.4). Our photonic quantum Hall system consisted of a twisted four mirror cavity nearly identical to the one used by Schine et al. [1], but made out of stainless steel instead of plastic, and with slightly different dimensions. In order to allow coarse adjusting of cavity length, one cavity half is fixed to a micrometer stage.

Measuring the Chern invariant requires taking images of the cavity output under controlled frequency and mode injections. To stabilize our cavity to allow for control of probe frequency, we use a Pound-Drever-Hall lock. One of the four mirrors is glued to a piezo, a piece of ceramic which expands when it receives voltage. This enables electronic feedback to lock the cavity to resonance. The feedback bandwidth of the piezo is small compared to the noise experienced by the cavity. To compensate for this, we lock the cavity to the laser at low frequencies, but lock the laser to the cavity at high frequencies.

To make the Chern number measurement, we tune slightly away from degeneracy and sweep across the Landau level. To stabilize the resonator modes, we only use angular momentum

$l = 3n$, where n is an integer. We are close enough to degeneracy that our modes mix, so three-fold symmetric modes that are linear combinations of the lowest Landau level naturally occur (see Figure 2.1). Because we tune the cavity slightly away from degeneracy while imposing a three-fold symmetry, instead of looking like the lowest Landau level in Figure 1.5, our actual lowest Landau level looks more like Figure 2.2.

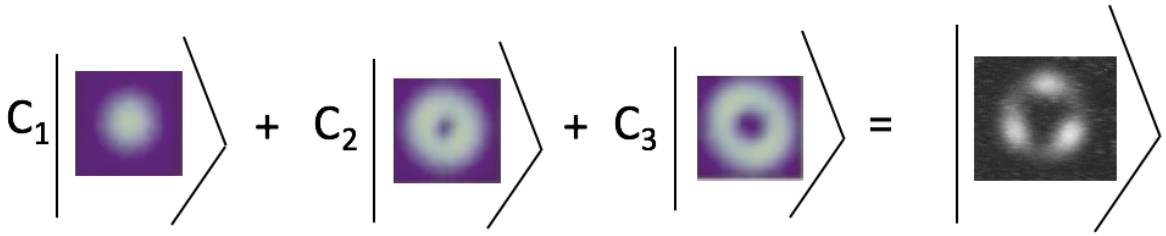

Figure 2.1: Our threefold symmetric modes appear at degeneracy, as linear combinations of Laguerre-Gauss modes of different angular momentums in the lowest Landau level.

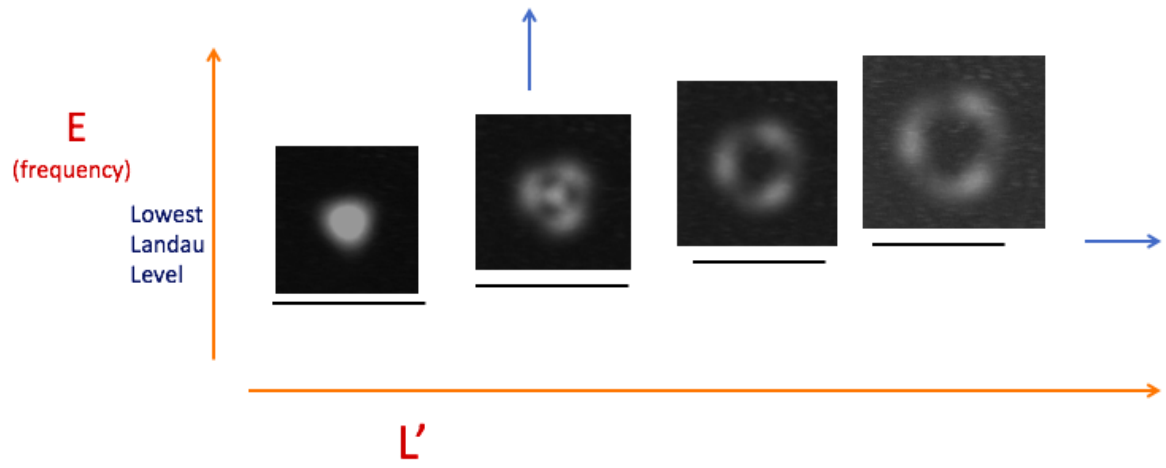

Figure 2.2: A cartoon drawing of the photonic Landau levels produced in our actual twisted four-mirror cavity system. Images are taken using our optical cavity setup. Brightness adjusted for clarity.

2.2 Imposing a Lattice and Lattice Site Injection

We impose a lattice on the transverse plane of our cavity (see Figure 1.3, and Figure 2.4), with a lattice spacing equal to the magnetic length, or equivalently, one half of the cavity waist.

Following section 1.4, we want to inject cavity modes at each lattice site i, and measure the complex-valued electric field out of the cavity at each site j, in order to find the band projectors at each matrix element, P^{μ}_{ij}. To inject a cavity mode at each lattice site, we use a DMD, or Digital Micromirror Device. A DMD is an array of thousands of tiny mirrors that can be switched on and off to allow for precise beam control. We created $r \times c$ holograms, one for each lattice site.

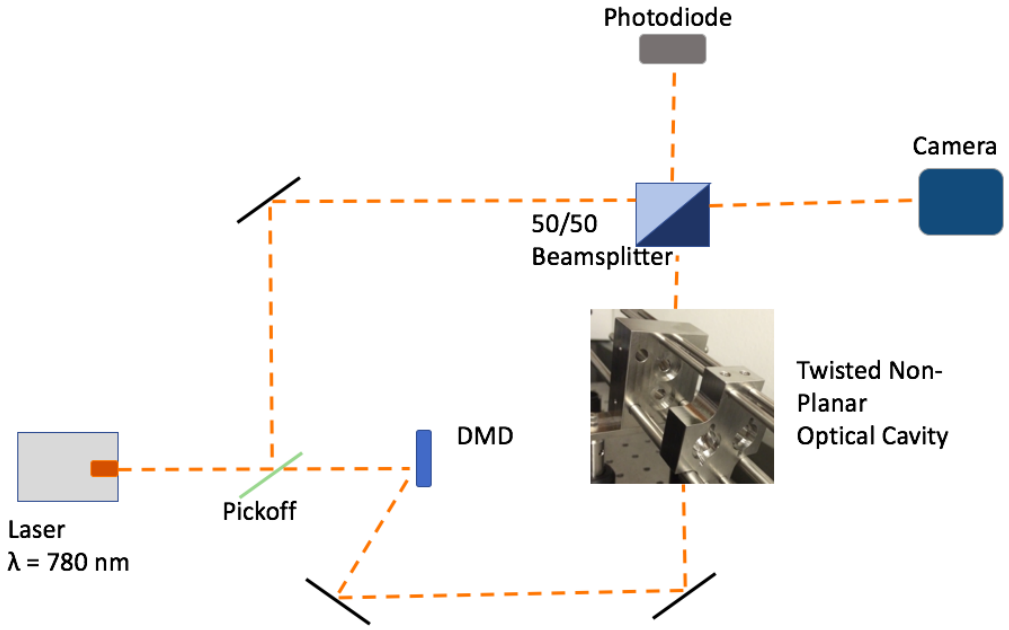

Figure 2.3: A cartoon diagram of our setup for measuring the Chern number of our twisted four-mirror optical cavity.

We display each hologram on the DMD, project laser light onto the DMD, send the first order diffracted beam (to take full advantage of the phase and amplitude control capabilities of DMDs [14]) through our optical cavity, and then image result with a camera (see Figure 2.3). The shutter of the camera is kept open while the laser sweeps over the lowest Landau level. In this way, we "integrate" over the entire band μ.

2.3 Output Grid Distortion

We found that the imposed lattice is distorted after going through the cavity. The injected lattice is an ordered, equally spaced square grid (see Figure 2.4a). However, a given lattice

site, r, c, in the cavity output, is expected to be the center of brightness of the reconstructed cavity mode injected at r, c. This results in an output lattice that is, particularly on the edges, significantly distorted (see Figure 2.4b). Fortunately, Kitaev's method for finding the Chern invariant is expected to work even in a disordered lattice [2, 13].

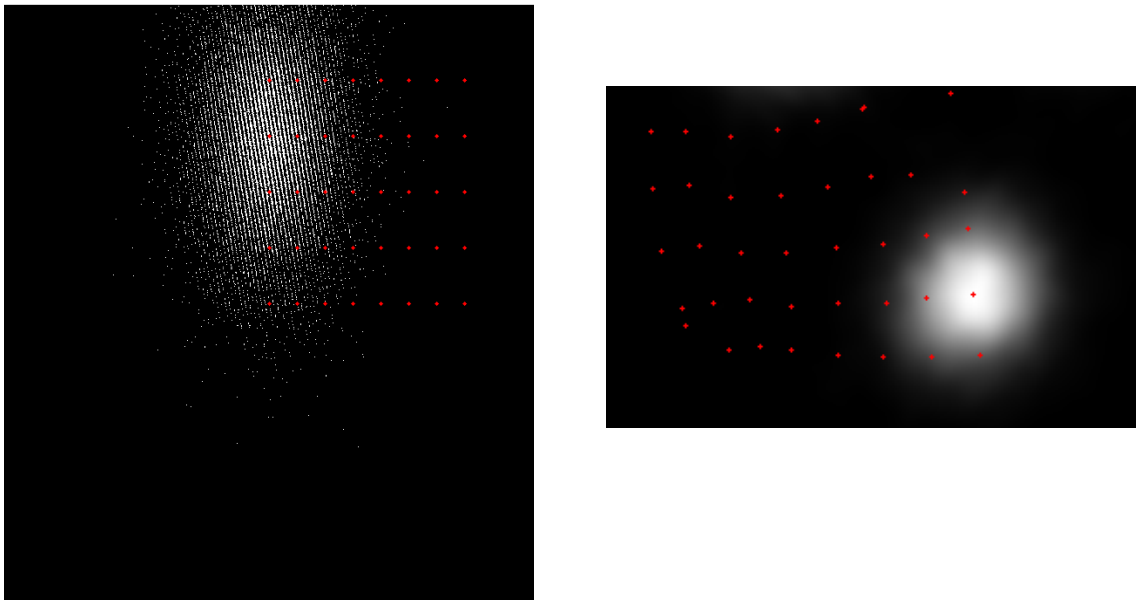

(a) (b)

Figure 2.4: (a) The hologram displayed on the DMD for injection at grid site (0,3) for a grid of size 8 by 5. The red dots show all of the lattice sites. A hologram was created centered on each lattice site site. Note that the grid looks rectangular in the figure, but because of the aspect ratio of the DMD mirror-pixels, it is actually square. (b) The absolute value of the electric field (after holographic reconstruction) for the hologram shown in Figure 2.4a. The actual mode is threefold symmetric, but only one of the three spots in the threefold symmetric mode is shown for clarity (an example of a holographic reconstruction with all three spots is shown in Figure 2.5a). The other two spots were unnecessary for the Chern invariant calculation, and so were masked away in the calculation. Each gridpoint is again shown in red. Note the lattice distortion, particularly on the edges, compared to the injected lattice shown in the hologram to on the left.

2.4 Holographic Reconstruction

The formalism we use to find the Chern number 1.9 requires finding the matrix value of the projector, $\langle i|P^{\mu}|j\rangle$. The projector matrix value $\langle i|P^{\mu}|j\rangle$ is equal to (up to a normalization

factor) the complex-valued electric field injected at site i and measured at site j. Simply imaging the cavity output only gives information on the electic field magnitude, and erases all phase information. To obtain phase information from our electric field, we make a plane wave heterodyne beam ($Ae^{i\vec{k}\cdot\vec{x}}$) by taking some of the beam before the DMD, and overlapping it with the cavity output (see Figure 2.3). We take images of the cavity modes alone and the heterodyne beam alone, and subtract these from the images of the cavity mode and the heterodyne beam together. Multiplying by the complex conjugate of our heterodyne beam gives us a reconstruction of the complex-valued electric field (see, as an example of the holographic reconstruction, Figure 2.5a).

$$
\begin{aligned}
E_{\text{cav}} &= m(\vec{x})e^{in(\vec{x})} \\
\text{Reconstructed Cavity Mode} &= |E_{\text{cav}} + Ae^{i\vec{k}\vec{x}}|^2 - (|E_{\text{cav}}|^2 + |Ae^{i\vec{k}\vec{x}}|^2) \\
&= m(\vec{x})e^{-in(\vec{x})}e^{i\vec{k}\cdot\vec{x}} + m(\vec{x})e^{in(\vec{x})}e^{-i\vec{k}\cdot\vec{x}}
\end{aligned}
$$

From this point, multiplying by $e^{i\vec{k}\vec{x}}$ and performing a Fourier transform, and filtering out the high frequency term ($e^{2i\vec{k}\vec{x}}$ will leave the complex-valued electric field, $m(\vec{x})e^{in(\vec{x})}$.

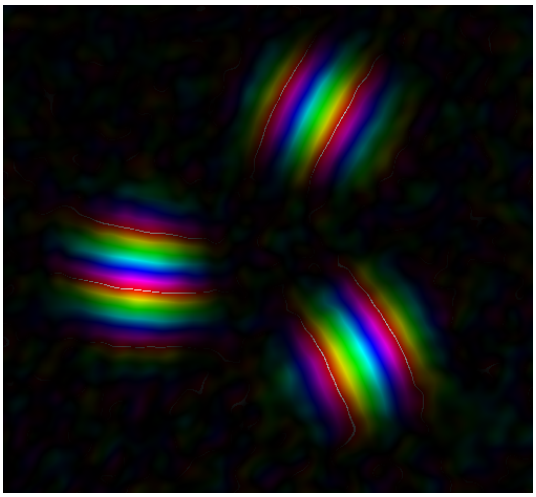

(a)

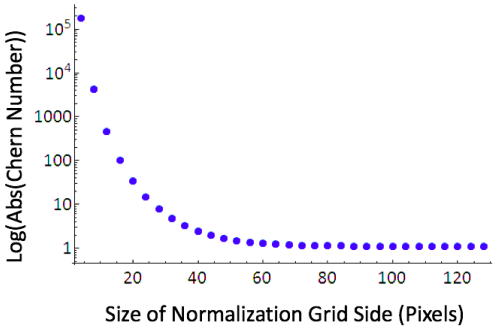

(b)

Figure 2.5: (a) Holographic reconstruction of a three-fold symmetric mode in our lowest Landau level. Brightness corresponds to magnitude, while color corresponds to complex phase. (b) A log plot of the magnitude of the Chern number (after normalization) compared with the normalization parameter, $N = M =$ Size of Normalization Grid (Pixels)

2.5 Normalization and Finding the Chern Invariant

After finding the projectors, it is fairly straightforward to follow the process outlined in section 1.4 to find the Chern number. The only thing remaining that we have not previously discussed normalization of the projector matrix elements. To force P_{ii}^{μ} to be real (as we can prove it should be, given $P^2 = P$), we multiply each projector P_{ij} by $P_{ii}^*/|P_{ii}|$. For instance, if P_{00} is $ze^{i\phi}$, this rotates every complex projector matrix element P_{0j} in the complex plane by $-\phi$. ϕ varies for each image, so this standardizes the phase referencing across images.

We also enforce another condition that must hold, $P_{ii} = \sum_j |P_{ij}|^2$ (which can be again proven from the fact that $P^2 = P$). We enforce this by making each projector P_{ij} equal to itself divided by $\sum_{n=-N}^{N} \sum_{m=-M}^{M} |P_{(r,c),(r,c)+(n,m)}| \cdot A_{nm}/A_{rc}$, where A_{nm} is the area in pixels of a gridpoint in a denser grid bounded by N, M, A_{rc} is the area in pixels of a gridpoint in the larger grid r, c, and i is the lattice site at r, c. The area elements allow us to change the range we sum n and m over. Given a fixed gridsize A_{nm}, we expect that the normalization sum we divide by should increase as we increase N and M to include more and more of the mode, and then plateau to the Chern number when the mode has been mostly included.

Chapter 3

Results and Discussion

3.1 Results

We make holograms for and take images of an 8 by 5 lattice, with lattice spacing equal to one half of the cavity waist. We obtain a Chern number for the lowest photonic Landau level equal to $1.08 - 0.12i$. This is approximately a 15% error from our anticipated Chern number of 1.

Changing a normalization parameters N and M changed the normalization constant, and hence the Chern number. A log plot showing the dependence of the magnitude of the Chern number on $N = M =$ Size of Denser Square Grid is shown in Figure 2.5. As expected, the Chern number decreases as the size of one side of the normalization square grid increases to include more of the mode pixels, plateauing near 1.

We remake our holograms to have a lattice spacing equal to one fourth of the cavity waist, and improve our normalization process by using the output (distorted) grid spacings as A_{rc}, rather than the injected grid spacings. We find a Chern number for the lowest photonic Landau level equal to $0.93 - 0.10i$. This is again approximately a 15% error from our anticipated Chern number of 1.

3.2 Discussion

We expected to get a Chern number of 1 for the lowest Landau level (given that we expect the lowest Landau level to be completely filled), and we measured 1 with a 15% error. We expect to get even closer to 1 by moving the injected mode to larger displacements from the center in order to eliminate unwanted interference between mode portions caused by the three-fold symmetry of our system.

We also plan to impose an edge in our system by changing our frequency sweep to sweep over only part of the Landau level, effectively blocking the other Landau levels with a wall of infinite potential. We expect this wall will introduce a counter-propagating edge mode along the boundaries of our sweep range, and measuring the Chern number over our entire system including the counter-propagating edge mode should result in a Chern number of 0. This will be easy to implement with our existing experimental setup and will be a nice way to check our understanding of our system.

Bibliography

[1] Nathan Schine, Albert Ryou, Andrey Gromov, Ariel Sommer, and Jonathan Simon. Synthetic landau levels for photons. *Nature*, 534:671–675, 2016.

[2] Alexei Kitaev. Anyons in an exactly solved model and beyond. *Ann Phys*, 321:2–111, 2006.

[3] G. Gumbs and D. Huang. *Properties of Interacting Low-Dimensional Systems*. WILEY-VCH Verlag, 2011.

[4] D. Tong. *The Quantum Hall Effect: TIFR Infosys Lectures*. Centre for Mathematical Sciences, Cambridge, 2016.

[5] David J Griffiths. *Introduction to Quantum Mechanics*. Cambridge University Press, second edition, 2017.

[6] C.L. Kane. *Topological Insulators*. Elsevier B.V., 2013.

[7] M. V. Berry. Quantal phase factors accompanying adiabatic changes. *Proceedings of the Royal Society of London A: Mathematical, Physical and Engineering Sciences*, 392(1802):45–57, 1984.

[8] Shiing-Shen Chern. A simple intrinsic proof of the gauss-bonnet formula for closed riemannian manifolds. *Annals of Mathematics*, 45(4):747–752, 1944.

[9] D. J. Thouless, M. Kohmoto, M. P. Nightingale, and M. den Nijs. Quantized hall conductance in a two-dimensional periodic potential. *Phys. Rev. Lett.*, 49:405–408, Aug 1982.

[10] S. M. Girvin R. E. Prange. *The Quantum Hall Effect*. Springer-Verlag, 1987.

[11] Charles Kittel. *Introduction to Solid State Physics*. John Wiley and Sons, Inc., 8th edition, 2005.

[12] F. D. M. Haldane. Model for a quantum hall effect without landau levels: Condensed-matter realization of the "parity anomaly". *Phys. Rev. Lett.*, 61:2015–2018, Oct 1988.

[13] Ruichao Ma, Clai Owens, Aman LaChapelle, David I. Schuster, and Jonathan Simon. Hamiltonian tomography of photonic lattices. *ArXiv*, 1607.05180, 2016.

[14] P. Zupancic. *Master's Thesis: Dynamic Holography and Beamshaping using Digital Micromirror Devices*. Ludwig-Maximilians-Universitat Munchen, 2013.